



**HAL**  
open science

# Finite difference simulations of seismic wave propagation for the 2007 Mw 6.6 Niigata-ken Chuetsu-Oki earthquake: Validity of models and reliable input ground motion in the near field

Hideo Aochi, Ariane Ducellier, Fabrice Dupros, Mickael Delatre, Thomas Ulrich, Florent de Martin, Masayuki Yoshimi

## ► To cite this version:

Hideo Aochi, Ariane Ducellier, Fabrice Dupros, Mickael Delatre, Thomas Ulrich, et al.. Finite difference simulations of seismic wave propagation for the 2007 Mw 6.6 Niigata-ken Chuetsu-Oki earthquake: Validity of models and reliable input ground motion in the near field. *Pure and Applied Geophysics*, 2013, 170 (1-2), pp.43-64. 10.1007/s00024-011-0429-5 . hal-00980238

**HAL Id: hal-00980238**

**<https://brgm.hal.science/hal-00980238>**

Submitted on 17 Apr 2014

**HAL** is a multi-disciplinary open access archive for the deposit and dissemination of scientific research documents, whether they are published or not. The documents may come from teaching and research institutions in France or abroad, or from public or private research centers.

L'archive ouverte pluridisciplinaire **HAL**, est destinée au dépôt et à la diffusion de documents scientifiques de niveau recherche, publiés ou non, émanant des établissements d'enseignement et de recherche français ou étrangers, des laboratoires publics ou privés.

1 Submitted to special issue of PAGEOPH (Jan 2011), revision on July 2011, accepted on Sept  
2 2011.

3

4 Finite difference simulations of seismic wave propagation for the  
5 2007 Mw 6.6 Niigata-ken Chuetsu-Oki earthquake: Validity of  
6 models and reliable input ground motion in the near field.

7

8 Hideo Aochi<sup>1</sup>, Ariane Ducellier<sup>1</sup>, Fabrice Dupros<sup>2</sup>, Mickael Delatre<sup>1</sup>, Thomas Ulrich<sup>1</sup>, Florent  
9 de Martin<sup>1</sup>, and Masayuki Yoshimi<sup>3, 1</sup>

10

11 <sup>1</sup> Natural Risks and CO<sub>2</sub> Storage Safety Division, Bureau de Recherches Géologiques et  
12 Minières, Orléans, France

13 <sup>2</sup> Digital Information Services, Bureau de Recherches Géologiques et Minières, Orléans,  
14 France

15 <sup>3</sup> Geological Survey of Japan, National Institute of Advanced Industrial Science and  
16 Technology, Tsukuba, Japan

17

18

19 **Abstract**

20 Finite difference simulations of seismic wave propagation are performed in the Niigata area,  
21 Japan, for the 2007 Mw 6.6 Niigata-ken Chuetsu-Oki earthquake at low frequencies. We test  
22 three 3D structural models built independently in various studies. First aftershock simulations  
23 are carried out. The model based on 3D tomography yields correct body waves in the near  
24 field, but later phases are imperfectly reproduced due to the lack of shallow sediment layers;  
25 other models based on various 1D/2D profiles and geological interpretation provide good site  
26 responses but generate seismic phases that may be shifted from those actually observed. Next,  
27 for the mainshock simulations, we adopt two different finite source models that differ in the  
28 near-field ground motion, especially above the fault plane (but under the sea) and then along  
29 the coastline. Each model is found to be calibrated differently for the given stations. For  
30 engineering purposes, the variations observed in simulated ground motion are significant, but  
31 for seismological purposes, additional parameter calibrations would be possible for such a  
32 complex 3D case.

33

34

35

## 36 **1. Introduction**

37           The 2007 Mw 6.6 Niigata-ken Chuetsu-oki earthquake occurred on 16 July slightly off  
38 of the northwest coastline of the Japanese mainland (Figure 1). The hypocentral depth is  
39 about 10 km and the fault mechanism is reverse, causing no significant surface rupture.  
40 Although modern structures incurred little significant damage, the event did shut down the  
41 Kashiwazaki-Kariwa nuclear power plant located above the inferred fault plane, which  
42 induced changes in the seismic hazard evaluation criteria applied to nuclear power plants.  
43 This earthquake's mechanism is quite complex and remains uncertain despite the dense  
44 observation network in operation (cf. Aoi *et al.*, 2008). The main reason for this is that the  
45 subsurface structure is so complex that commonly used algorithms based on a 1D structure  
46 model are unable to accurately determine aftershock locations (Kato *et al.*, 2008, 2009;  
47 Shinohara *et al.*, 2008). Immediately after the mainshock, high acceleration levels measured  
48 on seismic records along the coast tended to indicate that the fault orientation was northwest  
49 dipping, despite the fact that the geological structure would indicate a southeast dipping fault.  
50 However on the basis of aftershock observations obtained from arrays deployed for one  
51 month after the mainshock, the interpretation that predominantly emerges is that the major  
52 part of faulting is southeast dipping (Kato *et al.*, 2009). Multisegment models are inferred  
53 from the InSAR observations (Aoki *et al.*, 2008; Nishimura *et al.*, 2008), and the possibility  
54 of rupture transfer between multisegment models is also dynamically simulated (Aochi &  
55 Kato, 2010). Thus understanding this earthquake is a seismologically challenging problem,  
56 and it is worth ascertaining how well we can reproduce the ground motion using the known  
57 seismological information for this earthquake.

58           The basic concept behind the seismic hazard evaluation is to be able to predict ground  
59 motion under a given situation (cf. Douglas & Aochi, 2008). As the time series analyses are  
60 increasingly called on in studying nonlinear soil-structure interaction in engineering

61 seismology, the need is ever greater to provide the (input) ground motion quantitatively from  
62 seismological observations. Recent progress in numerical simulation and computational  
63 resources enables us to theoretically simulate ground motions at high frequencies up to  
64 several Hz by taking into account a complex source description and heterogeneous material  
65 parameters. However the frequency limit still stands at around 0.5 - 1 Hz when comparing  
66 with the observed data. Well-known, successful examples can be cited for the 1995 Hyogo-  
67 ken Nanbu (Kobe), Japan, earthquake or the 2004 Parkfield, California, earthquake (cf.  
68 Pitarka *et al.*, 1998; Sasetyan, 2007). Both examples feature very shallow strike-slip faulting,  
69 relatively better studied than the fault mechanism for the 2007 Chuetsu-Oki earthquake we  
70 are dealing with in this paper. In any case, we believe it important to demonstrate how  
71 seismological insights serve to reproduce the ground motions in such difficult and complex  
72 cases.

73 In this paper, to study the validity of 3D subsurface structure models, we begin with  
74 simulations of the aftershocks, considered as point sources. We thence move on to the  
75 mainshock simulation using different finite source models provided by some seismological  
76 inversion studies. We compare the simulated ground motions with the records obtained on the  
77 permanent networks in terms of the waveforms and response spectra. In this paper, our aim is  
78 not to tune up the parameters to obtain the best model, but rather to analyze each model in  
79 detail and discuss how we can procure reliable input ground motion in the near field.

80

## 81 **2. Numerical Simulation Methodology**

82 All the simulations in this paper are carried out using the finite difference method  
83 based on the staggered grid with 4<sup>th</sup> order in space and 2<sup>nd</sup> order in time (Aochi & Madariaga,  
84 2003, Dupros *et al.*, 2008, references therein). The finite fault is approximated by a series of  
85 point sources in space (Olsen, 1994; Graves, 1996) and an arbitrary source time function can

86 be considered at each point. How material heterogeneity dealt with is considered a crucial  
87 issue in the finite difference scheme (cf. Moczo *et al.*, 2002; 2007). In this study, we follow  
88 Graves (1996) by averaging the material parameters, since the material interface is not always  
89 precisely defined at the FD grids we used.

90 We define our physical model volume as 110 km (EW) x 120 km (NS) x 30 km  
91 (depth). We use a grid spacing of  $\Delta s = 200$  m and a time step of  $\Delta t = 0.01$  sec for most of the  
92 simulations; in some cases, we calculate with  $\Delta s = 100$  m and  $\Delta t = 0.005$  sec, and  $\Delta s = 75$  m  
93 and  $\Delta t = 0.0035$  sec are used to check the convergence of simulations. For all cases, ten finite  
94 difference grids are added at each edge as a Perfectly Matched Layer absorbing boundary  
95 (Collino & Tsogka, 2001; Komatitsch & Martin, 2007). Thus, the numerical dimension is 570  
96 x 620 x 160 = 56 million grids for  $\Delta s = 200$  m, 1120 x 1220 x 310 = 423 million for  $\Delta s = 100$   
97 m and 1356 x 1716 x 429 = 1 billion for  $\Delta s = 75$  m. The calculation duration is 60 seconds.  
98 The upper frequency limit in the simulations is usually estimated as  $f_{\max} = V_{\min} / (5\Delta s)$ , where  
99  $V_{\min}$  denotes the minimum wave velocity in the structural model being used (Levander, 1988).  
100 Based on several tests using different grid spacings and filter frequency ranges, we find it  
101 empirically to be a quite useful parameter.

102 Our simulation procedure is illustrated schematically in Figure 2. The input files both  
103 for the structure and the source need to be handled with care. For the structure, we read the  
104 original files provided by different studies and assign the material property at each grid in our  
105 simulation program. For the source models, however, we format the source files prior to the  
106 simulations after carefully ascertaining how the inversions have been achieved. Since the  
107 synthetic near-field ground motion is quite sensitive to the source description in time and  
108 space, in order to reproduce the ground motions using the source models inverted from the  
109 observations, we must understand exactly how they are solved in terms of the Green's  
110 function being used and detailed source time description (cf. Aochi *et al.*, 2011).

111           The numerical dimension is not overly large, compared to some advanced simulations  
112 of wave propagation using finite difference methods (cf. Olsen *et al.*, 2009; Furumura & Saito,  
113 2009). In order to be able to repeat several simulations for verification and calibration  
114 purposes, we improved time performance through a hybrid implementation using MPI  
115 (Message Passing Interface) and threads by OpenMP (Open Multi-Processing) (Aochi &  
116 Dupros, 2011). It takes 40-minute and an 8-hour runs for coarse and medium-sized grids  
117 respectively, on the 128 processors (16 nodes x 8 cores) on JADE at CINES, the French  
118 national computing centre. It takes about 18 hours for the finer grid on the 256 processors (32  
119 nodes x 8 cores, namely 32 MPI sub-domains x 8 OpenMP threads).

120

### 121 **3. 3D Structural Models**

#### 122 **Geological Features**

123           In this section, we will be explaining three 3D structure models we use in this study.  
124 Their key features are summarized in Table 1, and the cross-sections of each model are shown  
125 on Figure 3. The flat part of this region and the folded hills in between, as well, are composed  
126 of thick sedimentary layers. Conversely, the surrounding mountains to the south and east are  
127 characterized by rocks. The complex lateral variations in basement structure along the NE-SE  
128 fault striking are ascribed to Miocene rifting during the opening stage of the Sea of Japan and  
129 the subsequent shortening of the crust (Okamura *et al.*, 1995; Kato *et al.*, 2009). Because the  
130 Mw 6.6 Chuetsu earthquake in 2004 occurred 30 km southeast of the area ruptured in 2007,  
131 this region is recognized as an active fracture zone or strain concentration zone, which had  
132 been identified through structural geology (Okamura *et al.*, 1995) and GPS observations  
133 (Sagiya *et al.*, 2000). Because this area exhibits complex 3D structures, the velocity structure  
134 must be correctly reproduced if we are to generate sound synthetic ground motions.

135

## 136 **The ERI Model**

137           The first model (hereinafter referred to as the “ERI” model) is built by P- and S-wave  
138 travel time Double-Difference tomography from aftershock observations on land and at the  
139 sea bottom (Kato *et al.*, 2008; Shinohara *et al.*, 2009; Kato *et al.*, 2009). A relocated  
140 aftershock distribution is provided as well, based on the ERI model. The minimum grid  
141 interval is 3 km (N125°E) x 5 km (N35°E) x 3 km (vertical). The minimum S-wave velocity  
142 ( $V_s$ ) obtained is 866 m/s.

143

## 144 **The NIED Model**

145           The second model (hereinafter referred to as the “NIED” model) is taken from  
146 Fujiwara *et al.* (2009) and is available on the J-SHIS website (Japan Seismic Hazard  
147 Information Station: <http://www.j-shis.bosai.go.jp>). The area of interest is largely the same as  
148 Hikima *et al.* (2007), also based on Fujiwara *et al.* (2006). Hikima *et al.* (2007) associate the  
149 preliminary structural model with the seismic reflection results, calibrate the structure (layer  
150 depths) beneath each station by means of the observed H/V spectrum (1D tuning) and also  
151 tune up the structure along cross-sections between source and receiver, particularly for the  
152 aftershocks of the 2004 Chuetsu earthquake (2D tuning). The file (J-SHIS) provided is  
153 described in terms of depth to the layer boundaries at mesh nodes of 45” in longitude and 30”  
154 in latitude (the 3<sup>rd</sup> mesh for land planning in Japan), namely about a 1 km x 1 km mesh. It  
155 contains 32 layers between the surface and the basement characterized by an S-wave velocity  
156 ( $V_s$ ) of 3300 m/s, but many of these are not present in the region of concern. The minimum  
157  $V_s$  is set at 350 m/s.

158

## 159 **The GSJ Model**



160 The third model, referred to in this paper as the “GSJ” model, is presented in  
161 Sekiguchi *et al.* (2009). They improved the earlier NIED model (Fujiwara *et al.*, 2006) for the  
162 Niigata area by carefully calibrating layer depths and rock parameters based on seismological  
163 observations and taking into account the regional dependency of material parameters. The file  
164 (appended CD-ROM of Sekiguchi *et al.*, 2009) provides the depth of layer boundaries at mesh  
165 nodes of 0.00625 degrees longitude and 0.004167 degrees latitude, i.e., about a 0.5 x 0.5 km  
166 mesh. Model 2 designated in their CD-ROM contains 50 layers above the Moho. Because the  
167 parameters beneath the basement ( $V_s = 3300$  m/s) are not supplied, we have used those from  
168 their previous study in other regions, the central part of Japan (Sekiguchi & Yoshimi, 2010).

169

## 170 **Comparison**

171 The original features of each model are provided in the corresponding references.  
172 Figure 3 shows the cross-sections for these three models derived from the numerical  
173 simulations. We note that while there are many layers in the NIED and GSJ models, all of  
174 them are not always present at the finite difference grid point. We then interpolate the  
175 material parameters by averaging (Graves, 1996) instead of estimating precisely the interface  
176 plane between the finite difference grids (Moczo *et al.*, 2002). While uncertainties linked to  
177 the numerical processing remain on the scale of a calculation grid, the models used do  
178 adequately represent characteristic features in Figure 3. The three models are visually similar  
179 in terms of the shape of the basin structure. Although the tomography study (the ERI model)  
180 is carried out independently, it does detect the basin structure (low velocity zone) well. As the  
181 ERI model is inverted from dense observation data mainly above the aftershock area, the  
182 resolution toward the north ( $Y=20$  km) is not good enough to be comparable with the other  
183 two models. The NIED and GSJ models are similar, but the bedrock depth seems different:  
184 the NIED model is generally deeper.

185

## 186 **4. Aftershock simulations**

### 187 **Model settings**

188         In order to examine the structural models in detail, we begin by simulating some small  
189 earthquakes. We chose two aftershocks of the 2007 Niigata-ken Chuetsu-oki earthquake that  
190 were well located by *Kato et al.* (2008) and *Shinohara et al.* (2008) and also have mechanisms  
191 obtained by the F-net broadband seismograph network (<http://www.fnet.bosai.go.jp>). Table 2  
192 summarizes the source parameters. The hypocentral depths given by the two catalogues differ  
193 by a few kilometres, although the epicenters are relatively well determined. The seismicity  
194 distribution in this area is often shallower than that routinely obtained (cf., the progress report  
195 of the Japanese national project on the observation along the strained zone, MEXT, 2010).  
196 We impose a smooth bell-shaped source time function (cubic B-spline function) of a 0.5-  
197 second duration at the hypocenter (Figure 4), which is reasonable for events of Mw 4.4. We  
198 simulate these sources for each of the three geological models.

199         Before discussing the simulation results, a question may be raised concerning the  
200 quality of finite difference simulations. In Appendix, we have provided our synthetic  
201 comparisons between the finite difference and spectral element methods using the ERI model  
202 for the first aftershock. It is thus found that the numerical simulations are reliable enough to  
203 provide the ground motion under the given model and conditions.

204

### 205 **Near-Field Ground Motion**

206         Figure 4 shows the comparison at station KZK (F-net) using the three structural  
207 models, all of which are simulated with  $\Delta s = 100$  m. This station is located at a depth of 60 m  
208 on terrain characterized as rocky, not only locally but also regionally to a certain extent. In the  
209 simulations, the event origin times are set at 0. We align the observations for the origin time

210 reported by the relocated earthquake catalogue (Table 2). The seismograms are not filtered at  
211 this station. First we observe that the P-wave arrives simultaneously for all the cases (UD  
212 component), but the S-wave arrival does differ somewhat. The ERI model, for which the  
213 earthquakes are relocated, yields the best arrival time, whereas the other two models, NIED  
214 and GSJ, display a delay of a few seconds (EW and NS components). Then, the two models  
215 predict much longer and stronger ground shaking than observations in the later phases. This  
216 would tend to indicate that their S-wave structure might need to be better tuned up, supposing  
217 that the relocated earthquake parameters are correct here. For this KZK station, the ERI model  
218 appears to be better constrained, presumably thanks to their 3D tomography coverage from  
219 the source area to the station. However, we find that the EW component of the first aftershock  
220 (07/16) displays a clear discrepancy between the synthetics and the observation, even with  
221 ERI model, as the later phases are those that become dominant in terms of amplitude. This  
222 issue is not perfectly resolved and represents a common tendency for this aftershock along the  
223 coastline (NIG018 and KK as well). The synthetics do not properly account for the later  
224 phases, possibly due to the more complex layer that is shallower than the given resolution (3  
225 km in depth, see Table 1).

226

## 227 **The Regional Wave Field**

228 Figures 5 and 6 show the comparison at different stations for different structural  
229 models for Aftershocks 1 and 2 respectively. Each seismogram is aligned as was described  
230 above. The seismograms are filtered with a 0.1 -0.5 Hz band-pass filter and only the EW  
231 component is shown; the response spectra for 5 % damping are also compared. There are still  
232 difficulties in reproducing both arrivals and later phases in a satisfactory manner, since they  
233 must exhibit a correct velocity profile on the direct path (first arrivals) as well as in a larger  
234 surrounding volume for the later phases. In this sense, it is not possible to determine whether

235 one model is better than another at this stage insofar as none of them are perfect for a  
236 particular study.

237         However, some remarks can be made, also briefly summarized in Table 3. First, some  
238 models are seen to generate later phases that are too large at some stations, for example, the  
239 GSJ model at NIGH12. The first phase, on the other hand, is fairly accurately rendered by  
240 some models at most stations because the source and structure parameters are relatively well  
241 established. We note some time shift in phase among the simulations and/or with respect to  
242 the observation, at NIG004 and NIG025 among others, for example. This indicates that  
243 further improvement may be achieved both in source and structural parameters, but this is not  
244 this study's objective. Generally in the near field (cf., NIG018, NIGH11, NIG019, NIG017,  
245 NIG016, counter-clockwise), where the propagation path is relatively simple, the  
246 reproduction is quite good (especially Figure 6 for Aftershock 2). The response spectra  
247 indicate the validity of the average response around the given stations. The simulation of  
248 Aftershock 2 is found to be more consistent with the observation than that of Aftershock 1,  
249 for which the simulations underestimate the long-period portion of the spectra at the nearest  
250 station along the coast. This once again indicates that Aftershock 1 could afford further  
251 calibration, probably of the focal depth and/or local structure around the source. In the  
252 Kashiwazaki area in the simulation of Aftershock 2, station KZK (a rock site) is well  
253 reproduced by the ERI model, while NIG018 (a soil site) is rendered best by the GSJ model,  
254 reflecting local geological conditions.

255

## 256 **Discussion**

257         As already stated, the simulations are sometimes not as satisfactory for Aftershock 1.  
258 Reasons for this could be that the source parameters are not well constrained or the local  
259 structure for this earthquake is not precise enough. As the arrival times of the main phases are

260 fairly good in different directions, the earthquake location appears reliable. Our next step,  
261 then, was to invert Aftershock 1's focal mechanism using the ERI model and apply the  
262 neighbourhood algorithm so as to generate a wide range of parameters without prior  
263 information. After several trials using different stations and different components of the  
264 seismograms, we always obtain a focal mechanism of approximately (strike, dip, rake) =  
265 (181°, 65°, 84°), which differs from the reference solution only by 10 degrees. We may  
266 accordingly conclude that the focal mechanism obtained is stable. The remaining open  
267 question is: how is it possible to have only one component that does not fit well?

268

## 269 **5. Mainshock simulations**

### 270 **Finite source models and simulations in 1D layered models**

271 In this section, we chose two finite source models, both involving a southeast dipping  
272 reverse fault. Figure 7 shows the projection of the fault plane and the final slip obtained and  
273 Table 4 summarizes their characteristics. We used model B (southeast dipping) drawn from  
274 Aoi *et al.* (2008). The model initially obtained by Hikima and Koketsu (2007) was recently  
275 integrated into the work of Miyake *et al.* (2010). We found hypocentral locations only about 1  
276 km apart; however, due to differences in strike and dip, the discrepancy between the two fault  
277 planes is greater. Both models are analysed using available near-field strong ground motion.  
278 The only significant difference is that Hikima and Koketsu (2007) used the nearest station  
279 data (KK) at the Kashiwazaki-Kariwa nuclear power plant, while Aoi *et al.* (2008) do not.  
280 Note that the data at NIG018 seems to have been distorted by the strong liquefaction at the  
281 site, and the record at KZK is saturated for the mainshock. In Figure 8, we show the source  
282 time function for each model, which is not retrieved directly from their provided file but  
283 rather is based on our input file after changing the file format to make it compatible with our

284 code (e.g. Figure 2). This is important so as to verify our simulations and also for our  
285 subsequent discussion of how the strong ground motion is radiated.

286 We first entered these input files in the simple 1D structure and verified that the source  
287 model was properly taken into account. Aoi *et al.* (2008) introduced the moving source effect  
288 when calculating their Green's functions semi-theoretically. We approximated this effect  
289 numerically by means of 5 x 5 sub-sub-point sources distributed on each sub-fault in our  
290 finite difference simulation, as we already demonstrated in other earthquakes (e.g. Aochi *et al.*,  
291 2010). For this earthquake, we observe that the moving source effect is also visible at NIG004.  
292 Table 5 gives the 1D velocity structure models derived from the inversions. These are  
293 representative of their reference velocity models to a certain extent, but it should be borne in  
294 mind that the two inversions adopt different 1D velocity models independently calibrated at  
295 every station, that is, the wave field we simulate here does not simultaneously represent all  
296 the stations. We chose NIG004 and NIG016 for, as seen on Figure 9, the 1D structure from  
297 Aoi *et al.* corresponds better to NIG004 and that from Hikima & Koketsu to NIG016. The  
298 compared ground motions were filtered between 0.1 and 0.5 Hz and calculated with  $\Delta s = 200$   
299 m. The origin time is set at 10:13:22.16 (JST) for the observation, and the simulations start at  
300  $t=0$ . Our synthetic ground motion for the Aoi *et al.* model is consistent with the observation at  
301 NIG004. Note that their inversion uses only 14 seconds, consisting mainly of the S-wave.  
302 This confirms our implementation of the finite source models. At NIG016, the synthetic  
303 motion from Hikima & Koketsu reproduces the characteristic waveforms, especially for the  
304 vertical component, with time shift of a few seconds. Such a time shift is common in  
305 inversions, as the location of the hypocenter and the origin time are not always the same.  
306 These verifications not only confirm our numerical implementations but also reflect some of  
307 the inversion procedures.

308           We first carried out simulations in 1D layered models. The reason for this is that most  
309 seismological and seismic hazard applications still call on this simple structure except for a  
310 few well-known areas in the world, such as southern California, southeastern Japan and  
311 Taiwan. In practice, the two source models that were adopted are deduced using this  
312 approximation. It accordingly is worthwhile to observe the effects of a 3D structure with  
313 respect to the 1D layered models.

314

### 315 **Simulations in 3D structure models**

316           It is not at all evident that the combination of any 3D structure model with any finite  
317 source model obtained within a 1D layer model can coherently reproduce the observation,  
318 although this procedure is recommended to predict the ground motion for scenario  
319 earthquakes intended for use in quantitative seismic hazard studies. It is thus useful now to  
320 seek to obtain the characteristic ground motions at different stations and discuss the capability  
321 and limitations of the given models.

322           Figures 10 and 11 show the comparison of a number of synthetic ground motions and  
323 the observations at each station for both source models, bearing in mind the fact that the  
324 duration of the source process is approximately 15 seconds (Figure 8). The ground motions  
325 correspond to the EW component alone and are filtered between 0.1 and 0.5 Hz, because the  
326 comparison using this component is enough representative. The ERI model is simulated with  
327  $\Delta s = 200$  m and the others with  $\Delta s = 100$  m.

328           Let us examine the stations in the near field (NIG018, NIGH11, NIG019, NIG017,  
329 NIG016, counter-clockwise). The source model from Aoi *et al.* properly reproduces the  
330 waveforms for the first main phases (about 15 seconds) at NIG016 and NIG019, and the one  
331 from Hikima & Koketsu is well suited to NIG017. This coincidence implies that the 1D  
332 structural model used in their inversions may be briefly consistent along the concerned cross-

333 section. Looking at later phases, we also note that goodness of fit is influenced more by the  
334 structure than by the source. Both source models reproduce the later phases properly at  
335 NIGH11, NIG019, and NIG017 with the NIED and GSJ structures but not with the ERI  
336 structure. For NIG018, the three characteristic main pulses are clearly visible, especially in  
337 the combination of the NIED structure and the Hikima & Koketsu source model, though the  
338 amplitude is much smaller in the synthetics. An additional study of nonlinear soil dynamics  
339 could be conducted for this station using the synthetic seismograms as input ground motion,  
340 but this is beyond the scope of our study.

341         Now let us look at the stations at moderate distance (NIG025, NIG024, NIGH12,  
342 NIGH09, NIGH07, NIG011, NIG010, and NIG004). The ERI structure, for example,  
343 produces much larger later phases at NIG004, NIG025 and NIGH07, not noticeable in earlier  
344 comparisons of aftershocks (Figures 5 and 6), implying that the validity of structure should be  
345 evaluated taking into account the frequency content of the source time function. Furthermore,  
346 it is noted that the observed motion is much larger (spectra over all the frequency range) than  
347 any synthetics at NIG010 and NIG011, and this discrepancy is more obvious for the  
348 mainshock than for the aftershock. This indicates that the mainshock generates much larger  
349 surface waves than the aftershock.

350         In this section, we combine different source and structure models to simulate the  
351 ground motions. For the same reason already cited in the previous section for the aftershock  
352 simulations, it is impossible to determine whether one model is better than the others, for this  
353 depends on which aspect one is looking at, since no combination is currently perfect.

354

## 355 **6. Discussion**

356         The numerical simulations reflect the current level of seismological knowledge  
357 concerning this earthquake. For practical reasons, it is thus important to study the variations in



358 the calculated result from the standpoint of seismic hazard studies. It was predictable that the  
359 simulations for the mainshock would not fit the data well in terms of waveforms because the  
360 fault models are derived supposing some 1D structures: this may be the limit of our  
361 seismological knowledge. However, for engineering purposes, the variation of the simulated  
362 ground motions is meaningful. Figures 12 and 13 show the PGV (Peak Ground Velocity) map  
363 (different frequency ranges up to 0.5 Hz) for the three structural and two source models. Each  
364 source model is also calculated with the reference 1D velocity models (Table 5). As observed  
365 in the seismograms (Figures 10 and 11), the source model from Hikima & Koketsu yields  
366 stronger ground motion near the coastline rather than offshore; furthermore, the PGV  
367 generated from the model by Aoi *et al.* is centred along the blind fault trace. This latter feature  
368 is common for thrust fault earthquakes due to the geometry. In other words, it is confirmed  
369 that the model from Hikima & Koketsu integrates some complexity in the rupture process that  
370 is acquired particularly from the very near-source records such as the station at the  
371 Kashiwazaki-Kariwa nuclear power plant. On the other hand, different 3D structure models  
372 briefly give the similar characteristic. The expansion of the green area is consistent with the  
373 existence of low-velocity sediments beneath the Sea of Japan between Sado Island and the  
374 mainland as well as in the Niigata plain (see topographical map in Figure 3), which cannot be  
375 seen in 1D structure modelling. The amplification under the sea is stronger for the ERI  
376 structural model, which is the only model constrained from the OBS stations, although the  
377 shallow sediment layer under the sea is difficult to evaluate. Cirella *et al.* (2008) also obtained  
378 the finite source model by the joint inversion of strong motion and GPS data and show their  
379 forward modelling result in the 1D structure. Concerning the ground motion pattern above the  
380 fault plane, the model by Cirella *et al.* (2008) is closer to the one by Hikima & Koketsu used  
381 here. Kawabe and Kamae (2010) simulate the wave propagation in a 3D structure model  
382 provided by JNES (Japan Nuclear Energy Safety Organization, internal report, 2005) focusing

383 on the Kashiwazaki-Kariwa nuclear plant. They used a characterized, simple source model  
384 with three asperities and obtained the comparable synthetic ground motions (frequency range  
385 0.05 – 1.6 Hz), strongly affected by these asperities as well as by their local 3D structure. The  
386 JNES model may be more precise around this point of interest but remain essentially local in  
387 scope. Thus for the purposes of a regional discussion as provided in this paper, this model  
388 should be further compiled with other models.

389 We are also interested in other engineering parameters which characterize the ground  
390 motion. Figure 14 shows the comparison of PGV values (up to 0.5 Hz) at K-net and KiK-net  
391 stations. In terms of PGV (one of the most simple engineering parameters), we can confirm  
392 that the simulations are globally consistent with observations within this frequency range  
393 except for NIG018, and probably for other stations where later phases are not well modelled  
394 (e.g. NIG010 in the ERI structure). This is because the PGV is less sensitive to the details of  
395 the rupture process, being mainly affected by macroscopic parameters like fault location, fault  
396 geometry, rupture directivity, rupture velocity, and final magnitude. In this sense, both source  
397 models are suitable for simulating regional ground motion around the fault.

398 As already seen, this earthquake is an example in which it is difficult to quantitatively  
399 reproduce the waveforms. One possible reason is that the complex 3D structure masks the real  
400 features of this earthquake. Many kinematic inversions adopt the southeast dipping fault  
401 geometry, but this orientation is not the only one sustainable. Aochi and Kato (2010)  
402 demonstrate the possibility of a dynamic rupture transfer from a northwest dipping sub-fault  
403 to another southeast dipping sub-fault. The two models we used in this study differ in fault  
404 orientation, in the position of asperities and in rupture timing, and actually do not fit the same  
405 stations. Our study reported in this paper does not aim to calibrate the parameters, but the  
406 computing performance we have achieved will allow us to investigate further the source  
407 parameters in a 3D structure as well as to refine the structural models. We see that even the

408 subsurface structure obtained through fine tomography might not be sufficient to reproduce  
409 observed strong motions, nor those created through the use of both geologic and geophysical  
410 data. For some stations suffered from the strong ground motion (c.f. NIG018), it will be  
411 necessary to study by coupling with the nonlinear site effects at local level. We may conclude  
412 that a combination of tomography and data compiling in velocity structure modelling are  
413 called for.

414

## 415 **7. Conclusion**

416 Finite difference simulations of seismic wave propagation are carried out in the Niigata area,  
417 Japan, for the 2007 Mw 6.6 Niigata-ken Chuetsu-Oki earthquake at low frequencies. Some of  
418 the calculations are extended up to 1 Hz considering the minimum velocity in the medium of  
419 350 m/s. However we limit our discussion to 0.5 Hz throughout this study because of lack of  
420 precision in the model. We test three 3D structure models, all of which are built differently in  
421 various studies. From the aftershock simulations, it is seen that none of the models are  
422 uniform in their resolution and precision in this region, as the later phases are poorly  
423 reproduced in some more distant stations. The model based on 3D tomography (ERI model) is  
424 good enough for the near field in terms of body waves (arrival time), but its precision for  
425 shallow sediment layers is insufficient to reproduce the later phases properly, while the other  
426 models (NIED and GSJ models), based on various 1D/2D profiles and geological  
427 interpretation, work well for the site response, but do sometimes cause a time shift in phases.  
428 For the mainshock simulations, we adopt two different finite source models (Aoi *et al.*, 2008;  
429 Hikima and Koketsu, 2008), which differ in the near-field ground motion, especially above  
430 the fault plane (but under the sea) and also along the coastline. It is found that each model is  
431 calibrated differently for the given stations. For engineering purposes, the variation observed  
432 in simulated ground motion is significant, but for seismological purposes, further parameter

433 calibration is desirable and possible for such a complex 3D case using current high  
434 performance computing.

435

## 436 **Acknowledgments**

437 This work is carried out mainly in the framework of the French national ANR DEBATE  
438 project (DEvelopment of Broadband Accleration Timeseries for Engineers; 2009-2012). We  
439 thank all the colleagues for making available their numerical results: Drs. A. Kato, S. Aoi, H.  
440 Sekiguchi, K. Hikima and K. Koketsu. Many fruitful discussions were held with Profs. Raul  
441 Madariaga, Dr. Fabian Bonilla and Prof. Hiroshi Kawase, and Dr. Ken'ichi Tsuda from the  
442 DEBATE project. We thank Prof. Peter Moczo and Dr. Eiichi Fukuyama for improving the  
443 manuscript. We also express our appreciation for the data provided by K-net, KiK-net, and F-  
444 net of the National Research Institute for Earth Science and Disaster Prevention. HA thanks  
445 NIED for his invitation to Japan in October 2010. MY thanks AIST-GSJ for funding his visit  
446 to BRGM in 2009-2010. Part of the simulations were carried out at the super computing  
447 center (CINES) in France.

448

449

## 450 **References**

- 451 1. Aochi, H. and F. Dupros, Dynamic rupture propagation to seismic wave radiation in  
452 advance computing seismology, in the proceedings of the 1<sup>st</sup> International Workshop  
453 on Advances in High-Performace Computational Earth Sciences: Applications and  
454 Frameworks (IHPCES), Tsukuba, Japan, June, 2011.
- 455 2. Aochi, H., V. Durand and J. Douglas, Influence of super-shear earthquake rupture  
456 models on simulated near-source ground motion from the 1999 Izmit (Turkey)  
457 earthquake, Bull. Seism. Soc. Am., in press, 2011.

- 458 3. Aochi, H. and A. Kato, Dynamic rupture of crosscutting faults: A possible rupture  
459 process for the 2007 Mw 6.6 Niigata-ken Chuetsu-Oki earthquake, *J. Geophys. Res.*,  
460 115, B05310, doi:10.1029/2009JB006556, 2010.
- 461 4. Aochi, H. and R. Madariaga, The 1999 Izmit, Turkey, earthquake: Nonplanar fault  
462 structure, dynamic rupture process, and strong ground motion, *Bull. Seism. Soc. Am.*,  
463 93, 1249-1266, 2003.
- 464 5. Aoki, Y. M. Furuya and T. Kato, Coseismic deformation due to the 2007 Chuetsu-oki  
465 earthquake (Mw=6.8), *Earth Planets Space*, 60, 1075-1080, 2008.
- 466 6. Aoi, S., H. Sekiguchi, N. Morikawa and T. Kunugi, Source process of the 2007  
467 Niigata-ken Chuetsu-oki earthquake derived from near-fault strong motion data, *Earth*  
468 *Planets Space*, 60, 1131-1135, 2008.
- 469 7. Chaljub, E., P. Moczo, S. Tsuno, P. Y. Bard, J. Kristek, M. Kaser, M. Stupazzini, M.  
470 Kristekova, Quantitative comparison of four numerical predictions of 3D ground  
471 motion in the Grenoble Valley, France, *Bull. Seism. Soc. Am.*, 100, 1427-1455, 2010.
- 472 8. Collino, F. and C. Tsogka, Application of the perfectly matched absorbing layer model  
473 to the linear elastodynamic problem in anisotropic heterogeneous media, *Geophysics*,  
474 66, 294-307, 2001.
- 475 9. Day, S. M., J. Bielak, D. Dreger, R. Graves, S. Larsen, K. B. Olsen and A. Pitarka,  
476 Tests of 3D elastodynamic codes: Final report for Lifelines project 1A01, technical  
477 report for Pacific Earthquake Engineering Research Center, 2001.
- 478 10. De Martin, F., Verification of a spectral element method code for the Southern  
479 California Earthquake Center LOH.3 viscoelastic case, *Bull. Seism. Soc. Am.*, 101,  
480 doi:10.1785/0120100305, 2011.
- 481 11. Douglas, J. and H. Aochi, A survey of techniques for predicting earthquake ground  
482 motions for engineering purposes, *Surv. Geophys*, 29, 187-220, 2008.

- 483 12. Dupros, F., H. Aochi, A. Ducellier, D. Komatitsch and J. Roman, Exploiting intensive  
484 multithreading for the efficient simulation of 3D seismic wave propagation, in the  
485 proceeding of the 11th International Conference on Computational Science and  
486 Engineering, San Paulo, Brazil, 2008.
- 487 13. Fujiwara, H., S. Kawai, S. Aoi, N. Morikawa, S. Senna, N. Kudo, M. Ooi, K. X.-S.  
488 Hao, Y. Hayakawa, N. Toyama, H. Matsuyama, K. Iwamoto, H. Suzuki and Y. Liu, A  
489 study on subsurface structure model for deep sedimentary layers of Japan for strong-  
490 motion evaluation, Technical note of the National Research Institute for Earth Science  
491 and Disaster Prevention, Tsukuba, Japan, no. 337, 2009 (in Japanese).
- 492 14. Fujiwara, H., S. Kawai, S. Aoi, S. Senna, M. Ooi, H. Matsuyama, K. Iwamoto, H.  
493 Suzuki and Y. Hayakawa, A subsurface structure modelling of whole of Japan for  
494 strong-motion evaluation, in the proceeding of the 12<sup>th</sup> Japan Earthquake Engineering  
495 Symposium, 1466-1469, 2006 (in Japanese with English abstract).
- 496 15. Furumura, T. and T. Saito, An integrated simulation of ground motion and tsunami for  
497 the 1944 Tonankai earthquake using high-performance super computers, Journal of  
498 Disaster Research, 4, 2, 118-126, 2009.
- 499 16. Hikima, K. and K. Koketsu, Source process of the 2007 Chuetsu-oki earthquake  
500 inferred from far field waveforms and strong motions, Seismol. Soc. Japan, Fall  
501 Meeting, Abstract P1-085, 2007 (in Japanese).
- 502 17. Hikima, K., H. Suzuki, H. Miyake, T. Furumura and K. Koketsu, Construction of the  
503 3-D velocity structure model around Niigata district, Seismol. Soc. Japan, Fall  
504 Meeting, Abstract D22-01, 2007 (in Japanese).
- 505 18. Kato, A., E. Kurashimo, T. Igarashi, S. Sakai, T. Iidaka, M. Shinohara, T. Kanazawa,  
506 T. Yamada, N. Hirata and T. Iwasaki, Reactivation of ancient rift systems triggers

- 507 devastating intraplate earthquakes, *Geophys. Res. Lett.*, 36, L05301,  
508 doi:10.1029/2008GL036450, 2009.
- 509 19. Kato, A., S. Sakai, E. Kurashimo, T. Igarashi, T. Iidaka, N. Hirata, T. Iwasaki, T.  
510 Kanazawa and Groupe for the aftershock observations of the 2007 Niigataken  
511 Chuetsu-oki earthquake, Imaging heterogeneous velocity structures and complex  
512 aftershock distributions in the source region of the 2007 Niigataken Chuetsu-oki  
513 Earthquake by a dense seismic observation, *Earth Planets Space*, 60, 1111-1116, 2008.
- 514 20. Kawabe, H. and K. Kamae, Source modelling and 3D ground motion simulation of the  
515 2007 Niigataken Chuetsu-oki earthquake (Mj6.8), in the proceeding of the 13<sup>th</sup> Japan  
516 Earthq. Eng. Symposium, Tsukuba Japan, November 2010 (in Japanese with English  
517 abstract).
- 518 21. Komatitsch, D. and R. Martin, An unsplit convolutional perfectly matched layer  
519 improved at grazing incidence for the seismic wave equation, *Geophysics*, 72, SM155-  
520 SM167, 2007.
- 521 22. Kristekova, M., J. Kristek and P. Moczo, Time-frequency misfit and goodness-of-fit  
522 criteria for quantitative comparison of time signals, *Geophys. J. Int.*, 178, 813-825,  
523 2009.
- 524 23. Levander, A. R., Fourth-order finite-difference P-SV seismograms, *Geophysics*, 53,  
525 1425-1436, 1988.
- 526 24. Miyake, H., K. Koketsu, K. Hikima, M. Shinohara and T. Kanazawa, Source fault of  
527 the 2007 Chuetsu-oki, Japan, earthquake, *Bull. Seism. Soc. Am.*, 100, 384-391, 2010.
- 528 25. Moczo, P., J. Kristek, V. Vavrycuk, R. J. Archuleta, and L. Halada, 3D heterogeneous  
529 staggered-grid finite-difference modelling of seismic motion with volume harmonic  
530 and arithmetic averaging of elastic moduli and densities, *Bull. Seism. Soc. Am.*, 92,  
531 3042-3066, 2002.

- 532 26. Moczo, P., J. Kristek, M. Galis, P. Pazak and M. Balazovjech, The finite-difference  
533 and finite-element modelling of seismic wave propagation and earthquake motion,  
534 *Acta Physica Slovaca*, 57, 177-406, 2007.
- 535 27. Nishimura, T., M. Tobita, H. Yurai, S. Ozawa, M. Murakami, T. Yutsudo, M.  
536 Ishimoto, T. Umesawa, T. Toyofuku, S. Kawamoto, T. Amagai, M. Fujiwara, A.  
537 Suzuki, S. Enya, T. Sasaki, M. Yokokawa, S. Oomori, S. Tanoue, H. Ikeda, M.  
538 Nemoto, H. Suito, F. Hayashi, H. Une, M. Koarai and M. Tsuzawa, Crustal  
539 deformation and a preliminary fault model of the 2007 Chuetsu-oki earthquake  
540 observed by GPS, InSAR, and levelling, *Earth Planets Space*, 60, 1093-1098, 2008.
- 541 28. Okamura, Y., M. Watanabe, R. Morijiri, and M. Satoh, Rifting and basin inversion in  
542 the eastern margin of the Japan Sea, *Isl. Arc*, 4, 166–181, doi:10.1111/j.1440-  
543 1738.1995.tb00141.x, 1995.
- 544 29. Olsen, K. B., S. M. Day, L. Dalguer, J. Mayhew, Y. Cui, J. Zhu, V.M. Cruz-Atienza,  
545 D. Roten, P. Maechling, T.H. Jordan, and A. Chourasia, ShakeOut-D: Ground Motion  
546 Estimates Using an Ensemble of Large Earthquakes on the Southern San Andreas  
547 Fault With Spontaneous Rupture Propagation, *Geophysical Research Letters* **36**  
548 L04303, doi:10.1029/2008GL036832, 2009.
- 549 30. Pitarka, A. K. Irikura, T. Iwata, H. Sekiguchi, Three-dimensional simulation of the  
550 near-fault ground motion for the 1995 Hyogoken-nanbu, Japan, earthquake, *Bull.*  
551 *Seism. Soc. Am.*, 88, 428-440, 1998.
- 552 31. Sagiya, T, S. Miyazaki, and T. Tada, Continuous GPS array and present-day crustal  
553 deformation of Japan, *Pure and Applied Geophysics*, 157, 2303-2322, 2000.
- 554 32. Sasetyan, K., Caractérisation du spectre de réponse en champ proche d'une faille par  
555 simulation des mouvements forts du sol, PhD Thesis, University of Paris XI, France,  
556 2007.



- 557 33. Sekiguchi, H., M. Yoshimi, H. Horikawa, K. Yoshida, H. Suzuki, H. Matsuyama, M.  
558 Morino, F. Takizawa, and L. Ying, 3D subsurface structure model of the Niigata  
559 sedimentary basin, Geological Survey of Japan/AIST Annual report on Active fault  
560 and paleoearthquake researches, 9, 175-259, 2009 (in Japanese with English abstract).
- 561 34. Sekiguchi, H. and M. Yoshimi, Broadband ground motion reconstruction for the  
562 Kanto Basin during the 1923 Kanto earthquake, Pure and Applied Geophysics,  
563 doi:10.1007/s00024-010-0142-9, 2010.
- 564 35. Shinohara, M., T. Kanawaza, T. Yamada, K. Nakahigashi, S. Sakai, R. Hino, Y. Murai,  
565 A. Yamazaki, K. Obana, Y. Ito, K. Iwakiri, R. Miura, Y. Machida, K. Mochizuki, K.  
566 Uehira, M. Tahara, A. Kuwano, S. Amamiya, S. Kodaira, T. Takanami, Y. Kaneda  
567 and T. Iwasaki, Precise aftershock distribution of the 2007 Chuetsu-oki earthquake  
568 obtained by using an ocean bottom seismometer network, Earth Planets Space, 60,  
569 1121-1126, 2008.
- 570

571

572 **Appendix: Comparison between finite difference and spectral element**  
573 **methods**

574 Finite difference simulations are widely used for practical applications, but their  
575 quality is sometimes debated especially in the framework of synthetic benchmark tests (e.g.  
576 Day *et al.*, 2001; Chaljub *et al.*, 2010). As pointed out by many researchers, the finite  
577 difference scheme does not represent any interface correctly (free surface, faulting and  
578 material interface) but always gives an approximate solution. In this study, we do not deal  
579 explicitly with the interface plane in the numerical simulations even though the models  
580 initially supplied (the NIED and GSJ models) are defined by layers. As none of the three  
581 models are defined at the finite difference grids of calculation, estimating the material  
582 interfaces at given points requires further assumptions.

583 In this appendix, we are describing a comparative test using the finite difference as  
584 well as the spectral element methods (De Martin, 2011). We adopt the first example, namely  
585 the ERI structure model for the first aftershock. In the spectral element scheme, the material  
586 properties are interpolated at each of the GLL (Gauss-Lobatto-Legendre) points. The entire  
587 domain is uniformly meshed with hexahedra, constrained by the lowest S-wave velocity. The  
588 mesh is composed of 208,936 geometrical nodes, 196,425 hexahedra 1200 m in size in all  
589 directions and 16,757 quadrangles for absorbing boundaries by paraxial approximation  
590 different from our finite difference simulation. The polynomial order of the basic functions is  
591  $N = 4$ , and the total number of degrees of freedom is 46 million (including the redundant GLL  
592 at the interfaces between the CPUs). Also, the finite difference simulation here is carried out  
593 with a grid spacing of 200 m.

594           Figure A1 shows the comparison of the seismograms at NIG004 filtered in the  
595 frequency range between 0.1 and 0.5 Hz using the ERI model for Aftershock 1. Despite the  
596 completely different numerical procedures, the overall waveforms are well enough  
597 reproduced to allow the characteristics of the ground motion to be discussed. Figure A2  
598 shows the goodness-of-fit (GOF; Kristekova *et al.*, 2009) for the surrounding K-net stations  
599 as a function of epicentral distance. This criterion provides a succinct evaluation of how  
600 similar two signals are by a score assigned on a scale of 0 (poor) to 10 (excellent), and ranges  
601 higher than 6.5 and 8.5 are considered as good and excellent, respectively. It is observed that  
602 the GOF is better at closer distance because of the reduced influence of numerical dispersion  
603 and of little impact from absorbing conditions. In fact, the worst station, NIG002, which is  
604 qualified as fair (range 4.5 to 6.5), is very close to the model edge. Otherwise, it is confirmed  
605 that the simulations are fair enough both in amplitude and phase for the purpose of our  
606 discussions.

607 Tables

608 Table 1: Characteristics of the three different structural models. See the references in the text.

	ERI model	NIED model	GSJ model
Area covered	Around the area of the 2004 and 2007 earthquakes	All of Japan	Niigata area measuring about 200 km x 200 km
Principal data included	P- and S-wave tomography of the aftershock	Seismic reflection, geological interpretation, 1D tuning, 2D tuning	NIED model, geological interpretation, geophysical borehole data, 1D tuning
Given resolution	3 km (N35°E) x 5 km (N125°E) x 3 km at least	45'' in longitude and 30'' in latitude	0.00625 degrees in longitude and 0.004167 degrees in latitude
Vs minimum	866 m/s	350 m/s	400 m/s
Given property	Vp, Vs by point	Vp, Vs, ρ by layer	Vp, Vs, ρ by layer

609

610

611 Table 2: Source parameters of the aftershocks used in the simulations. The relocated  
 612 hypocentral parameters are based on Kato *et al.* (2008) and Shinohara *et al.* (2008). The focal  
 613 mechanisms are obtained routinely by F-net of NIED.

614

	Aftershock 1	Aftershock 2
Origin Time (JST)	2007/07/16 21:08:1.86	2007/07/18 16:53:5.01
Relocated hypocenter	37.4983°N, 138.6147°E, 15.413 km	37.4327°N, 138.5943°E, 16.880 km
Routinely obtained hypocenter	38.5088°N, 138.6297°E, 11 km	37.4418°N, 138.6153°E, 20 km
Mw	4.4	4.4
Focal mechanism (strike/dip/rake)	187°/54°/70°; 39°/41°/115°	39°/62°/95°; 208°/29°/80°

615

616

617 Table 3: Brief summary of characteristics of the three 3D structural models from the  
 618 aftershock simulations.

Model	Positive characteristics	Aspects to be improved
ERI	Synthetics at near-field rock site, especially in the south	Finer shallow structure, larger area
NIED	Synthetics at near-field soil site, good site response generally	Parameters in shallower soft layers, deep structure
GSJ	Synthetics at near-field soil site, good site response generally, similar to NIED	Same as above

619

620 Table 4: Characteristics of the finite fault models used in this study. Some parameters were  
 621 not specified by Hikima and Koketsu (2007), but we have supplied an estimated condition  
 622 indicated in the blank.

Model	Aoi <i>et al.</i>	Hikima & Koketsu
Reference	Model B from Aoi <i>et al.</i> (2008)	Hikima & Koketsu (2007)
Hypocentral location	37.54°N, 138.61°E	37.54014°, 138.62653°E
Focal depth	8.9 km	10 km
Fault geometry	Strike N49°E, dip 42°	Strike N38°E, dip 34°
Total seismic moment	1.62 x 10 <sup>19</sup> N.m	Not specified (1.02 x 10 <sup>19</sup> N.m)
Sub-fault number	15 (strike) x 12 (dip)	15 (strike) x 9 (dip)
Sub-fault size	2 km x 2 km	2 km x 2 km
Source time discretization	6 multi-windows	7 multi-windows
Rake	Free in each window	Free in each window
Source time function	A smoothed ramp function	Unknown (Ramp function)
Moving rupture effect	Yes	Unknown (No)

623

624

625 Table 5: 1D structure models used for the simulations of this study. (a) For Aoi's model, (b)  
 626 for Hikima & Koketsu's model.

627 (a)

Depth of the top of the layer [km]	Vp [m/s]	Vs [m/s]	Density [kg/m <sup>3</sup> ]	Q (attenuation)
0.0	4600	3090	2600	300
1.383	5900	3300	2700	300
13.632	6700	3800	2900	500
27.533	7700	4300	3250	500

628

629 (b)

Depth of the top of the layer [km]	Vp [m/s]	Vs [m/s]	Density [kg/m <sup>3</sup> ]	Q (attenuation)
0.0	2286.806	1020.620	2057.361	100
0.5	2570.792	1238.071	2114.158	100
1.0	2933.326	1517.943	2186.665	100
1.5	3091.167	1639.359	2218.233	100
2.0	3259.370	2094.144	2251.874	100
3.0	3682.388	2330.547	2336.478	100
4.0	4031.846	2490.645	2406.369	100
5.0	4308.815	2753.608	2461.763	100
6.0	4557.710	2891.243	2511.542	100
7.0	4763.741	3107.153	2552.748	100
8.0	5001.851	3403.074	2600.370	100
9.0	5375.374	3767.530	2675.075	100



10.0	5887.317	3403.074	2777.464	250
14.0	6517.827	3767.530	2903.565	250
20.0	6903.343	3990.372	2980.669	250
33.0	7587.204	4262.474	3113.777	250

---

630

631

632 Figure captions

633

634 Figure 1: Map of the area surrounding the 2007 Niigata Chuetsu Oki earthquake. The star  
635 represents the hypocentral location defined by Aoi *et al.* (2008). The black rectangle indicates  
636 the projection of the fault plane according to Aoi *et al.* (2008). The grey rectangle indicates  
637 the projection of the fault plane according to Hikima & Koketsu (2008). The pink dots  
638 represent the aftershocks relocated by Kato *et al.* (2008) and Shinohara *et al.* (2008) recorded  
639 over the space of one month immediately after the mainshock. The triangles and names are  
640 the seismograph stations from K-net, Kik-net, F-net and the Kashiwazaki-Kariwa nuclear  
641 power plant operated by TEPCO (KK).

642

643 Figure 2: Schematic representation of the simulation procedure.

644

645 Figure 3: Cross-sections of different 3D structure models in the numerical simulations. See  
646 the text for the details of each model, ERI, NIED and GSJ.

647

648 Figure 4: Comparison of synthetic and observed ground motion for the selected aftershocks  
649 (Table 2) at station KZK using three different structural models. All the seismograms are not  
650 filtered. The earthquake location and the given moment release function are shown at the top.  
651 Response spectra are calculated at the bottom for the waveforms up to 0.5 Hz.

652

653 Figure 5: Comparison of synthetic and observed ground motion for the first aftershock (Table  
654 2) at different stations for each structure model. The ground motion is calculated over 60  
655 seconds, then filtered between 0.1 and 0.5 seconds. The response spectra are also shown.

656

657 Figure 6: Figure 5: Comparison of synthetic and observed ground motion for the second  
658 aftershock (Table 2) at different stations for each structure model.

659

660 Figure 7: The two finite source models used in this study. Also see Table 4 for their  
661 characteristics.

662

663 Figure 8: Source time function prepared as the input file for the numerical simulations. Each  
664 panel is shown every 2 km, as are their inversions. Red lines indicate the dip component (rake  
665  $90^\circ$ ) and blue ones represent the strike component (rake  $0^\circ$ ) at each point.

666

667 Figure 9: Synthetic ground motions at NIG004 and NIG016 for the source models from Aoi *et*  
668 *al.* and Hikima & Koketsu, simulated in 1D structure models, respectively. The seismograms  
669 are filtered between 0.1 and 0.5 Hz.

670

671 Figure 10: Comparison of the synthetic ground motions at different stations for the Aoi source  
672 model of the mainshock using the three different 3D structure models. The component is  
673 East-West. The waveforms are filtered between 0.1 and 0.5 Hz.

674

675 Figure 11: Comparison of the synthetic ground motions at different stations for the Hikima &  
676 Koketsu source model of the mainshock using the three different 3D structure models. The  
677 component is East-West. The waveforms are filtered between 0.1 and 0.5 Hz.

678

679 Figure 12: Map of peak ground velocity (PGV) for each component (x: east-west, y: north-  
680 south, z: up-down) and the source model from Aoi *et al.* The seismograms are filtered up to  
681 0.5 Hz.

682

683 Figure 13: PGV map for the source model from Hikima & Koketsu.

684

685 Figure 14: Comparison of horizontal (geometric mean) PGV for six simulations (see also  
686 Figures 11 and 12). X symbols represent the observed values.

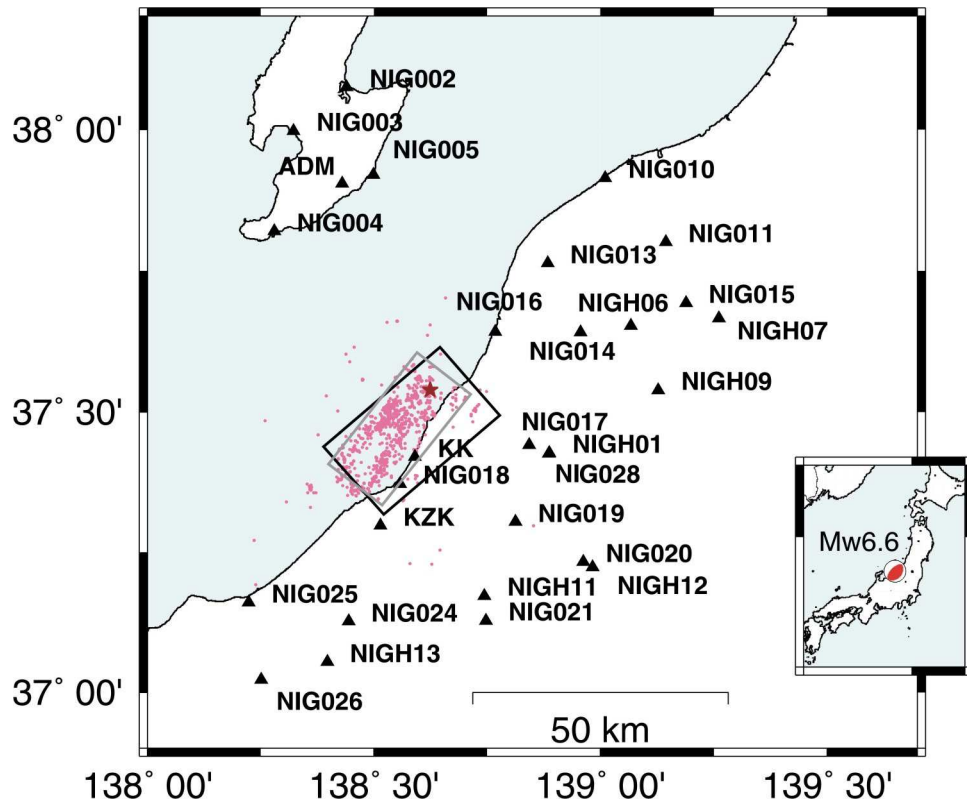
687

688 Figure A1: Comparison of synthetic seismograms at NIG004 calculated using the finite  
689 difference and spectral element methods. The structure is the ERI model and the source is  
690 Aftershock 1. The signals are filtered between 0.1 and 0.5 Hz.

691

692 Figure A2: The goodness-of-fit between the two simulations at the surrounding K-net stations.  
693 The seismograms are filtered between 0.1 and 0.5 Hz, and the scores for both amplitude (left)  
694 and phase (right) are shown for each component. The stations are aligned versus epicentral  
695 distance. The reference for the score is taken for the spectral element method. The coherence  
696 between two signals is excellent for a range of 8.5-10, good for 6.5-8.5 and fair for 4.5-6.5.

697 Figure 1 :



698

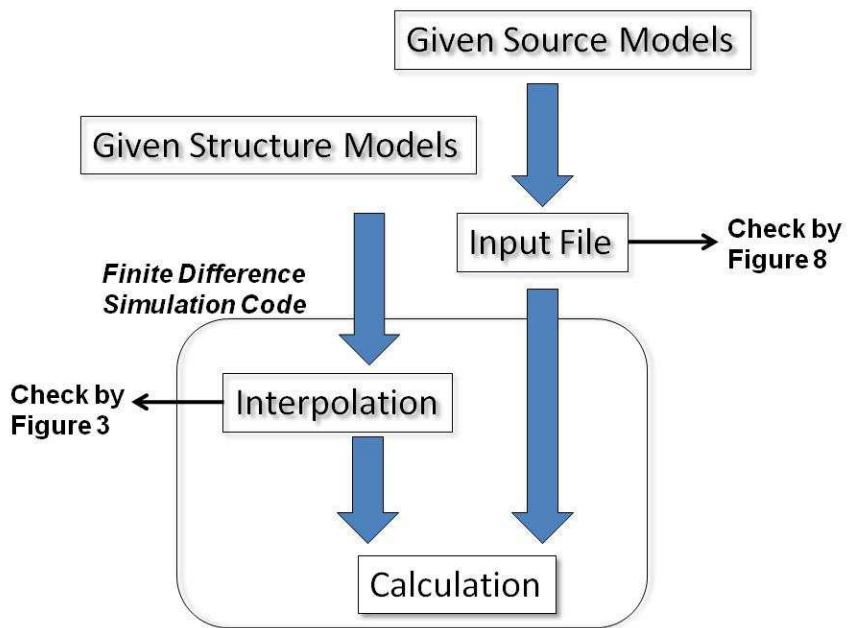
699

700 Figure 2:

701

702

## Simulation procedure

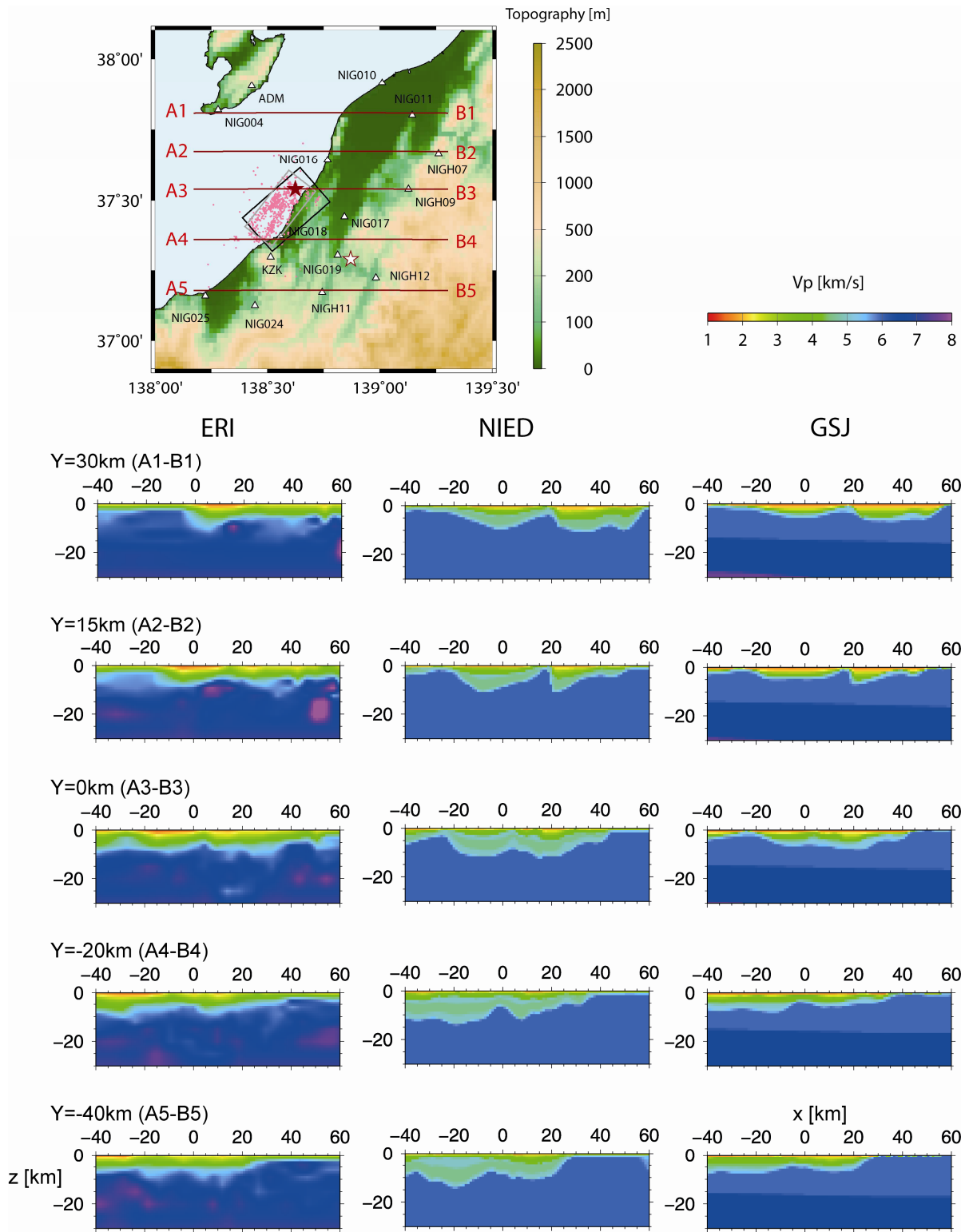


703

704

705

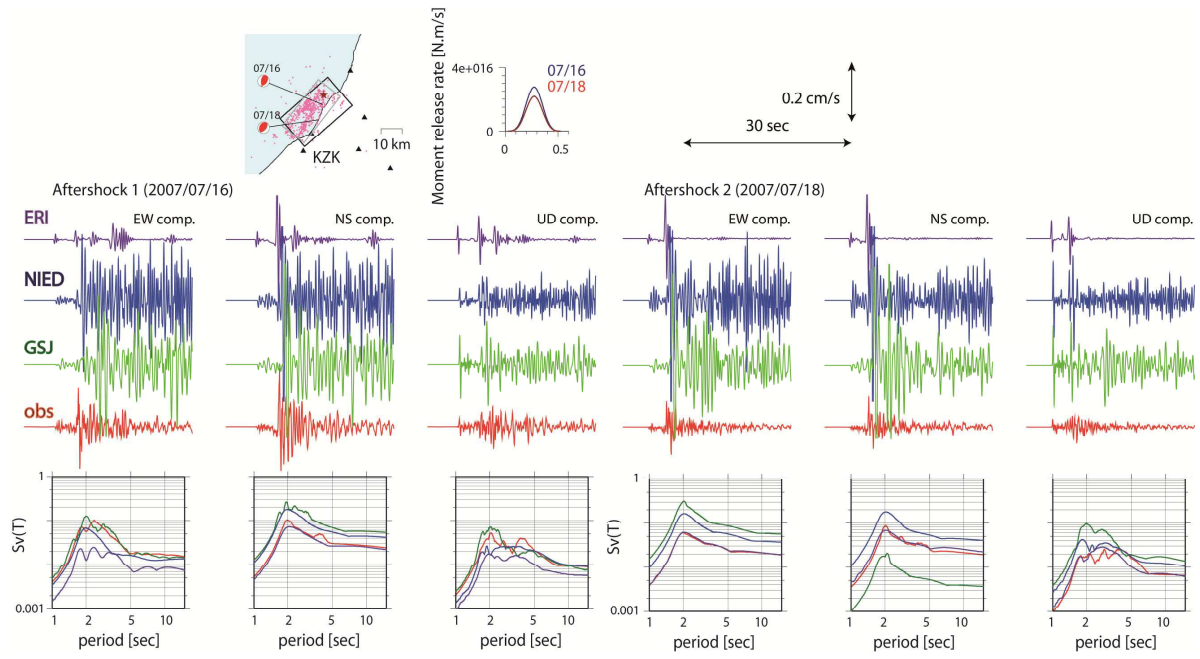
706 Figure 3:



707

708

709 Figure 4 : (revised)



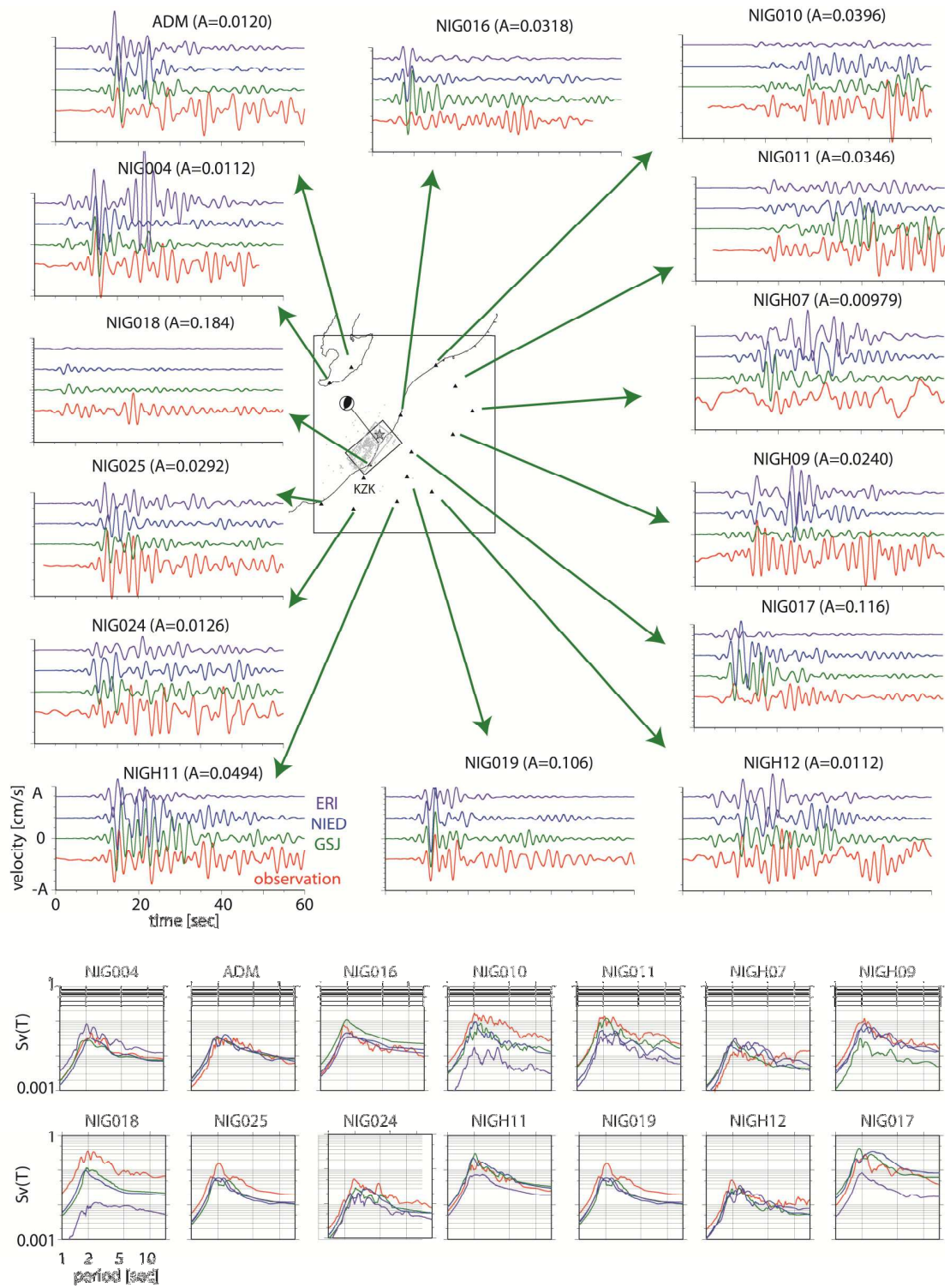
710

711

712



713 Figure 5:

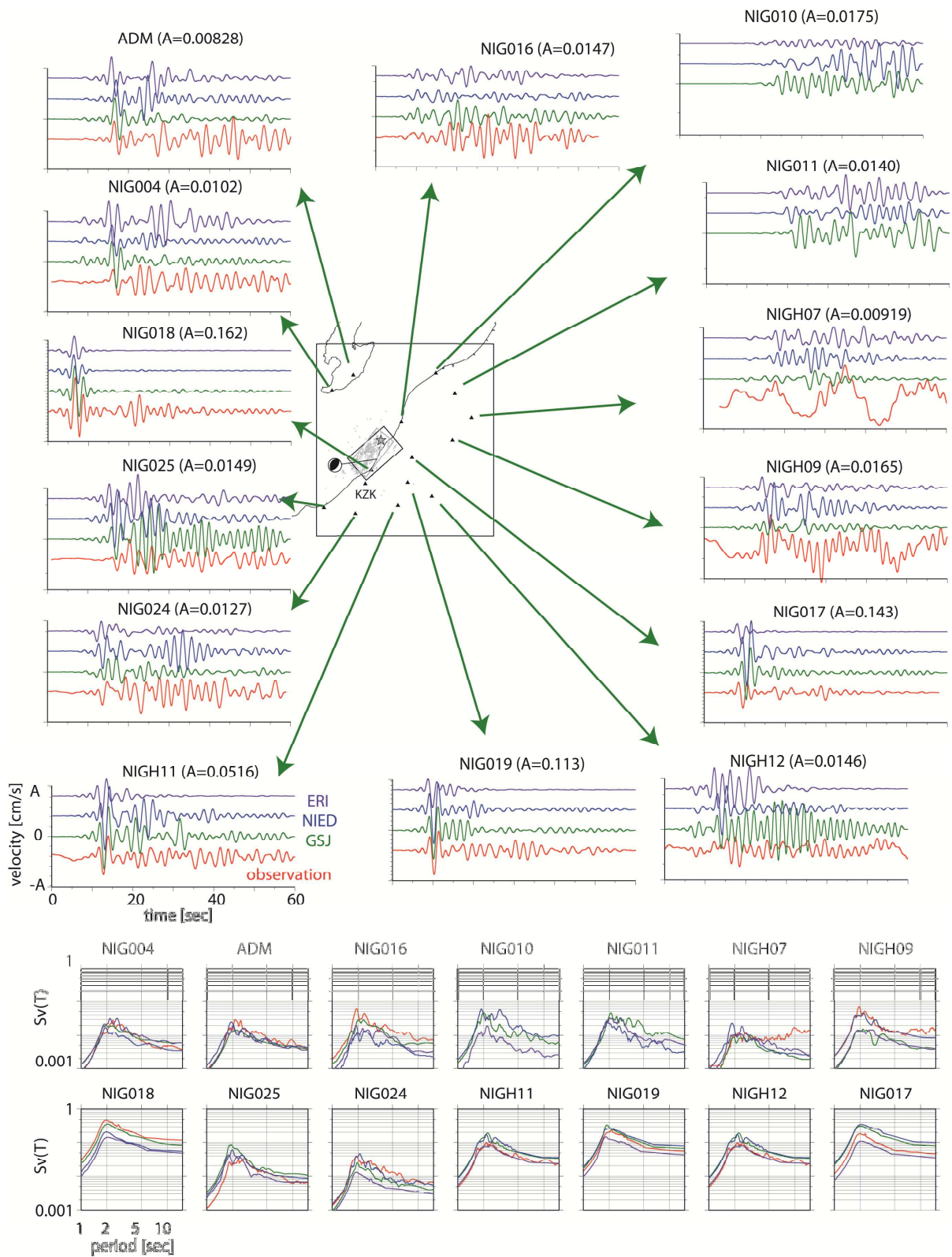


714

715

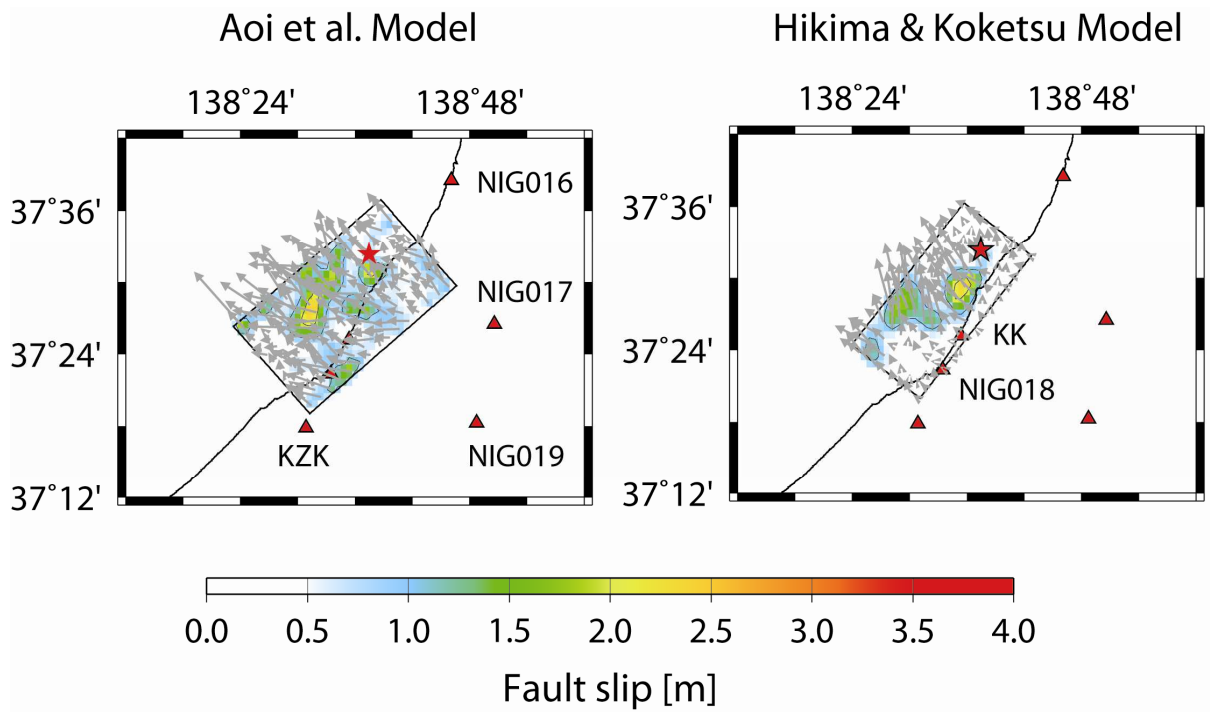
716

717 Figure 6:



718

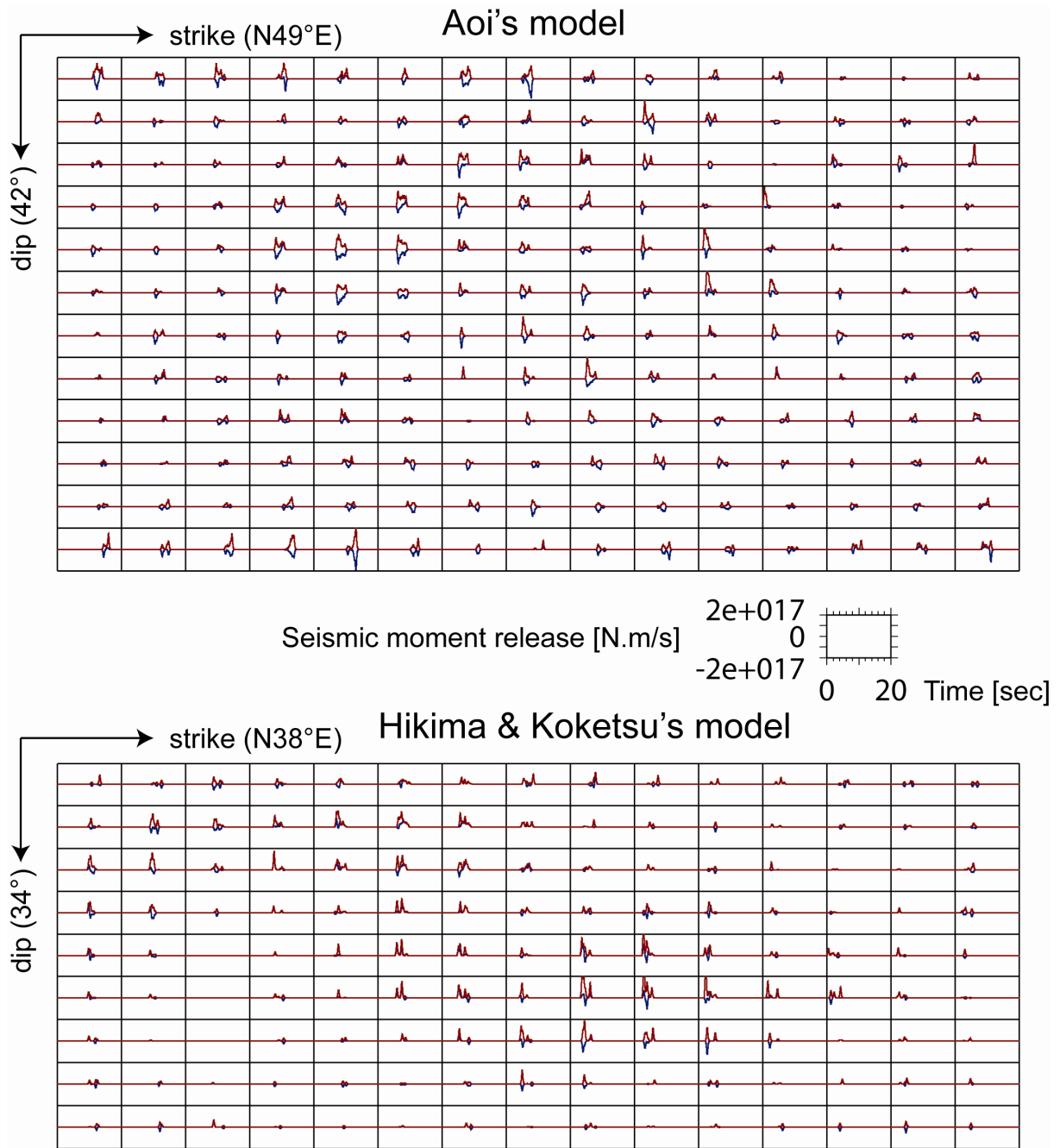
719 Figure 7:



720

721

722 Figure 8 :

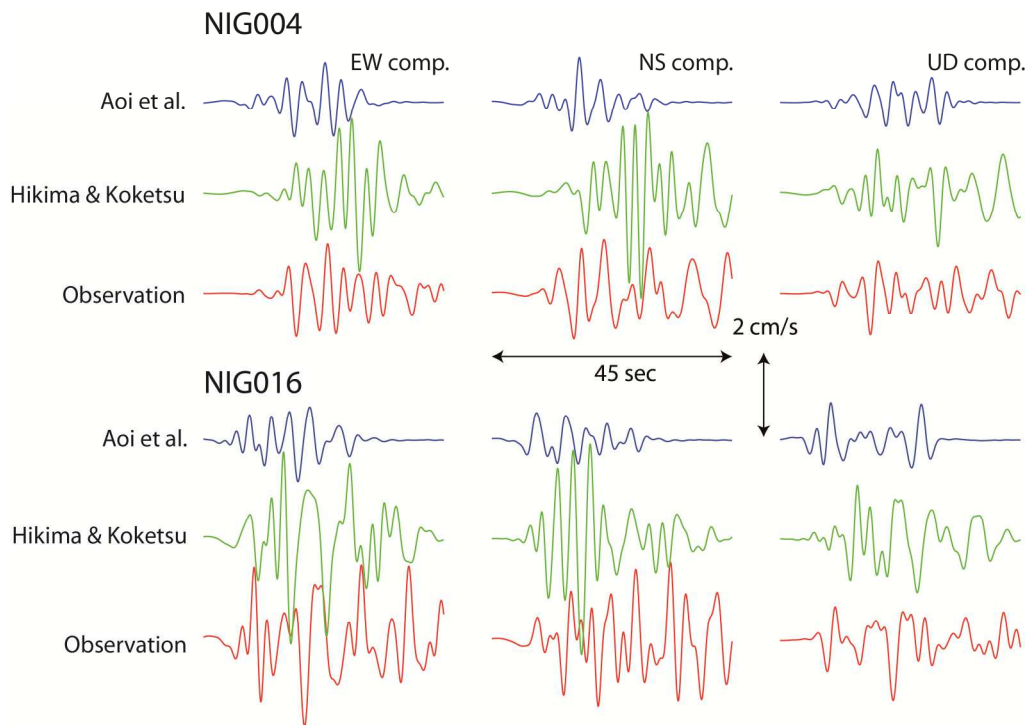


723

724

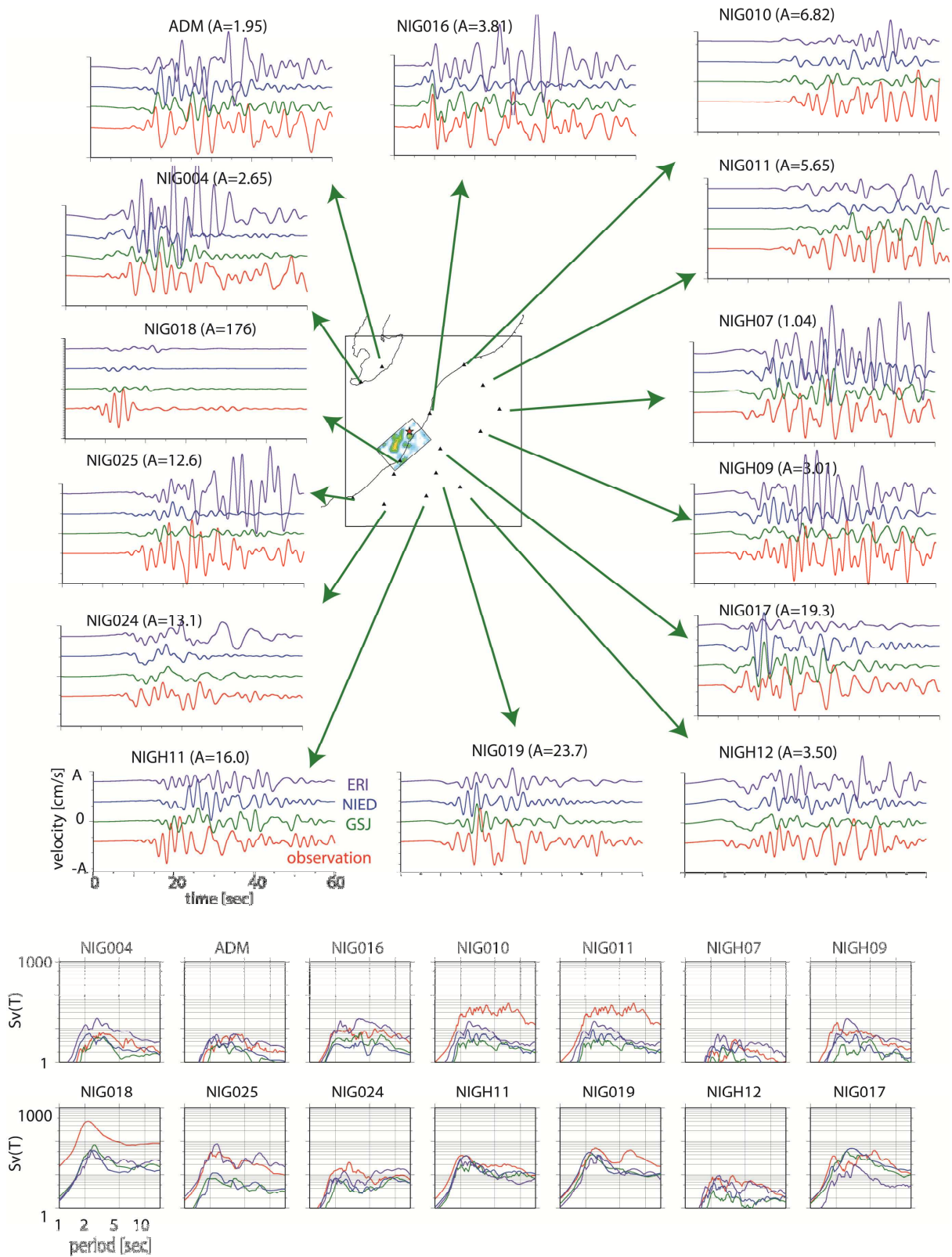
725

726 Figure 9 :



727

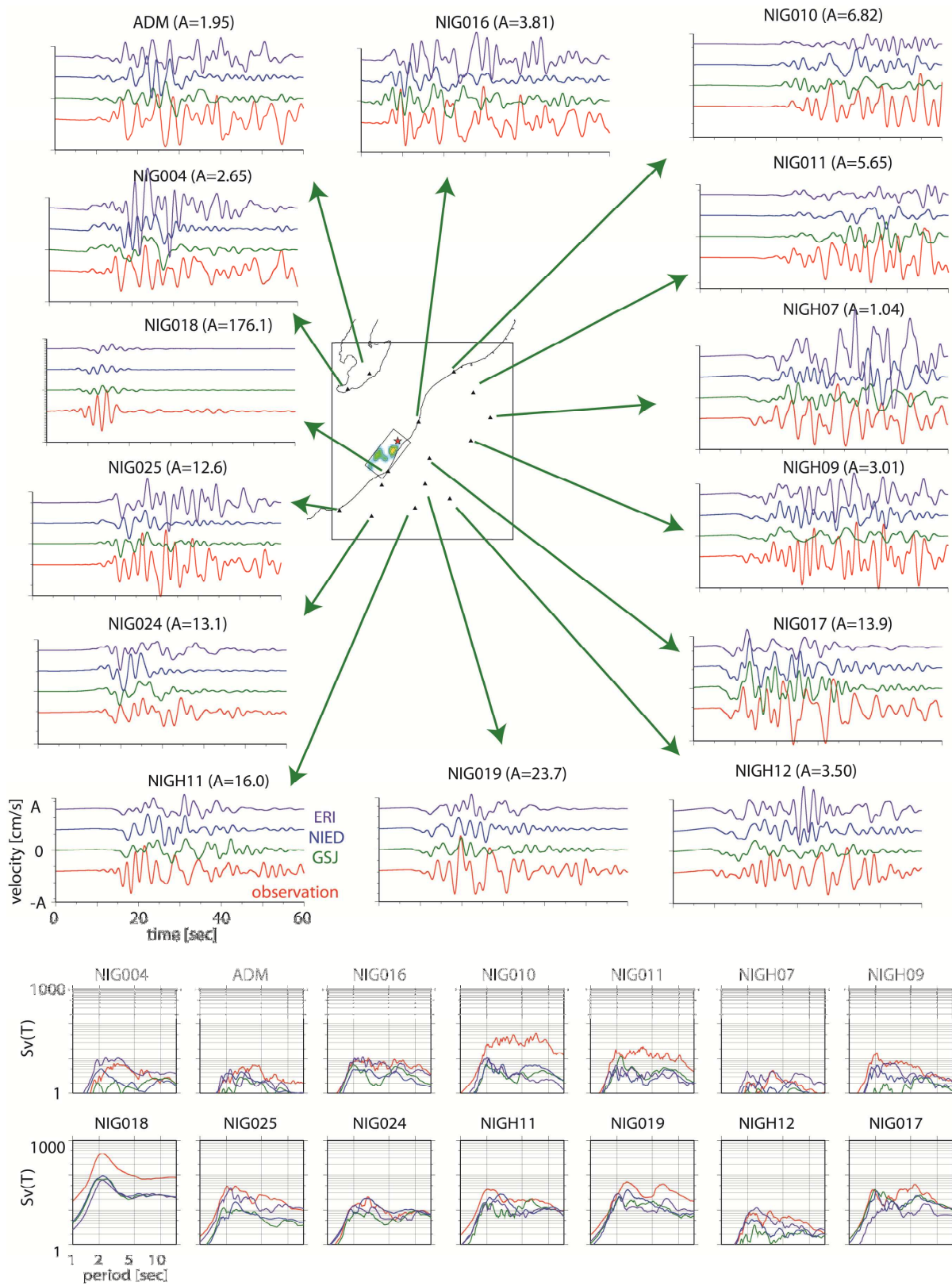
728 Figure 10 :



729

730

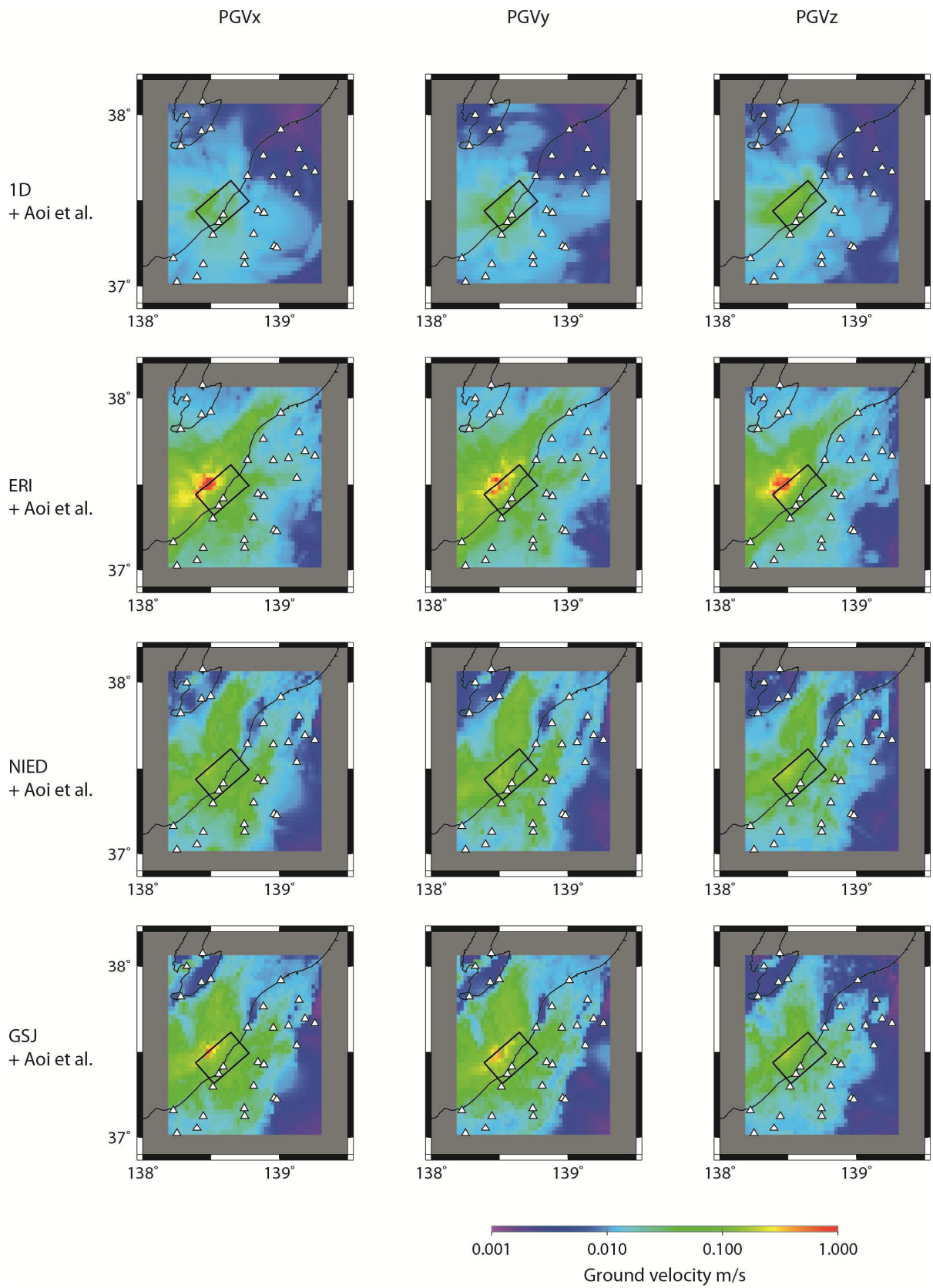
731 Figure 11



732

733

734 Figure 12 : (revised)

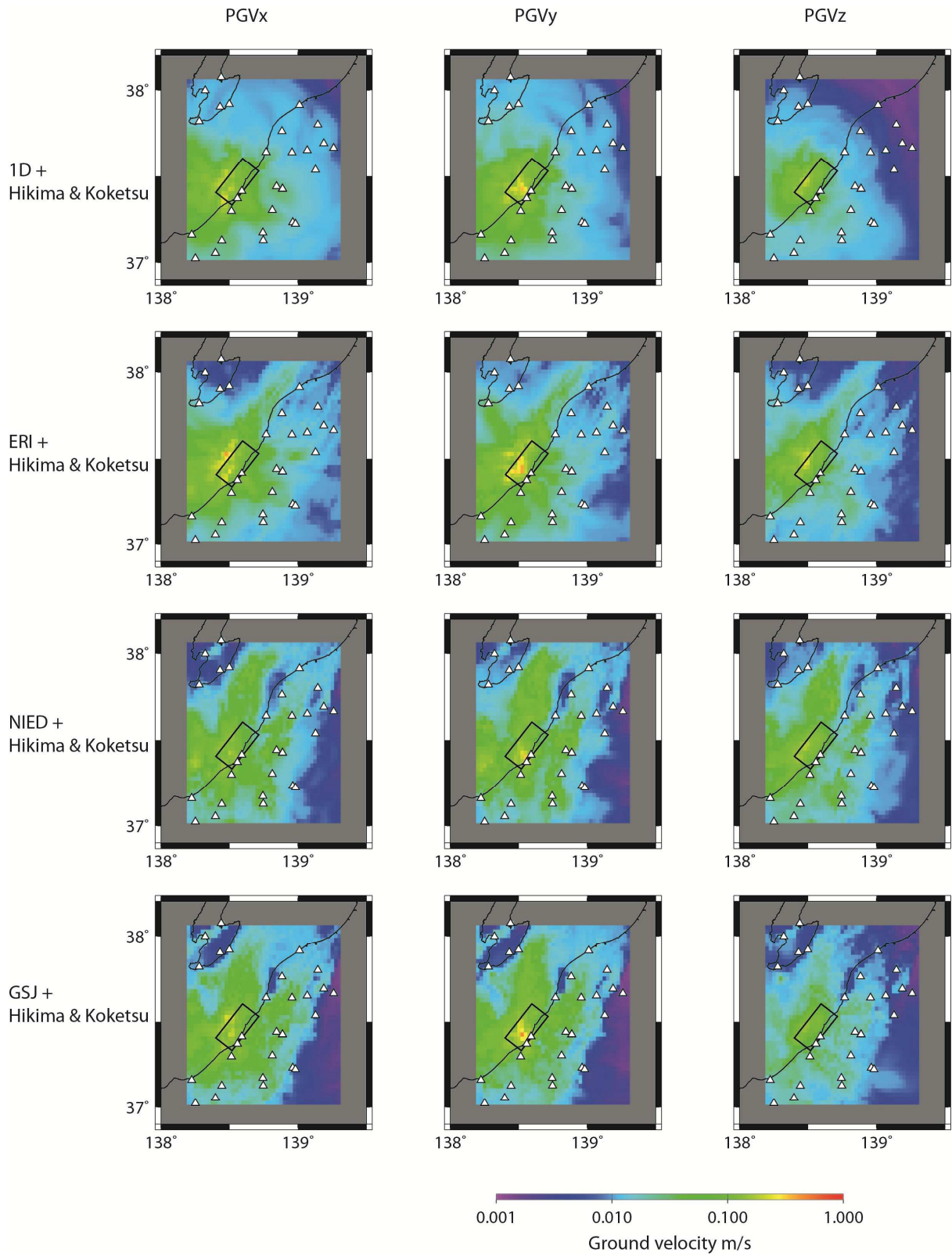


735

736



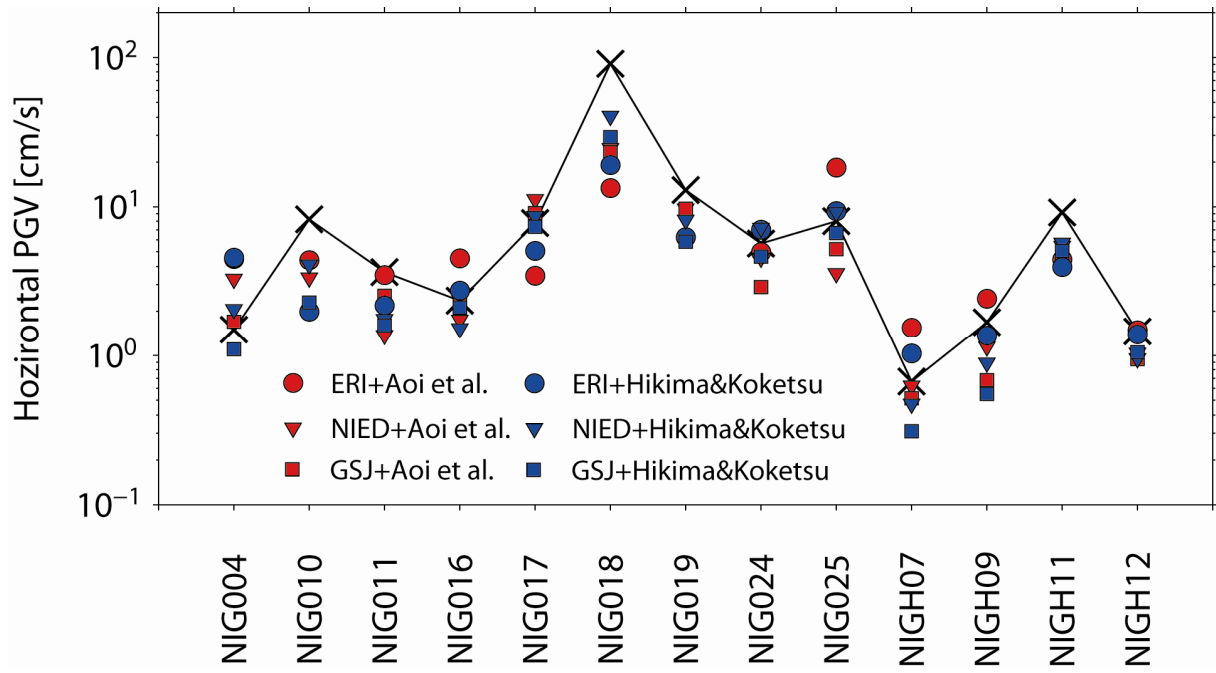
737 Figure 13 :



738

739

740 Figure 14 :

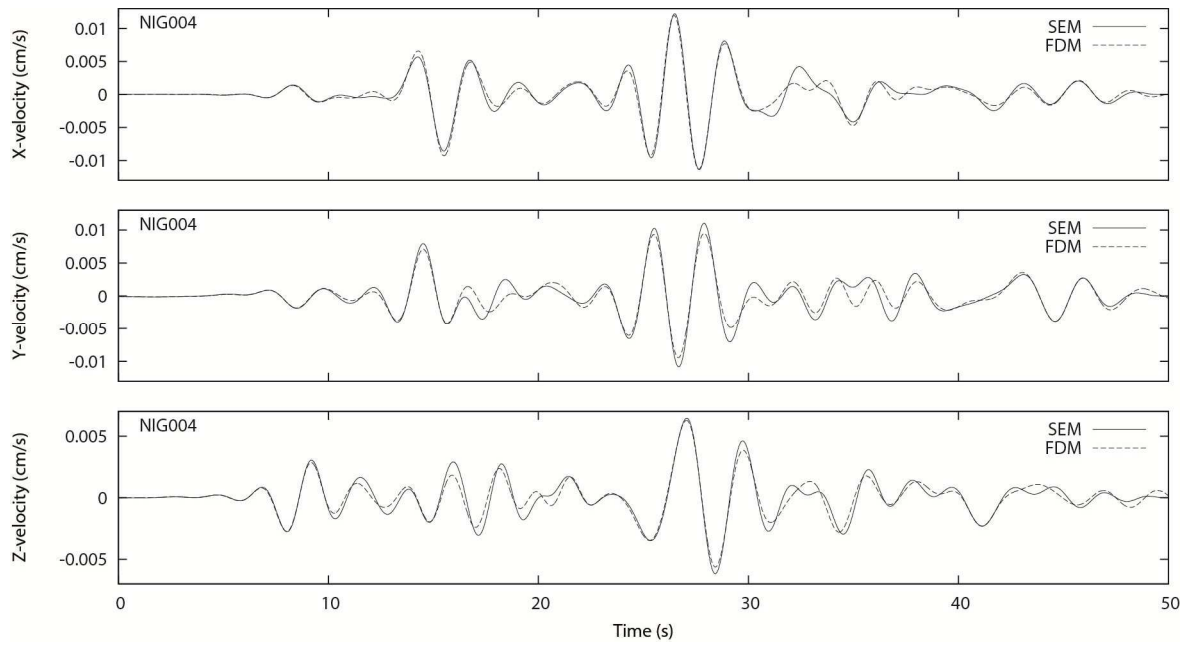


741

742

743

744 Figure A1 :

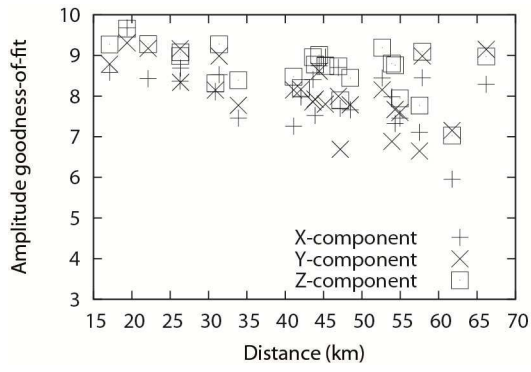


745

746

747

748 Figure A2 :



749

750

